

Younes Oulahou

Ph.D. student
Moulay Ismail University of Meknes
Faculty of sciences
Morocco

Youssef Elguennouni

Ph.D
Moulay Ismail University of Meknes
Faculty of sciences
Morocco

Mohamed Hssikou

Associate Professor
Sultan Moulay Slimane University
Polydisciplinary Faculty- LRPSI
Morocco

Jamal Baliti

Associate Professor
Sultan Moulay Slimane University
Polydisciplinary Faculty- LRPSI
Morocco

Mohammed Alaoui

Full Professor
Moulay Ismail University of Meknes
Faculty of sciences
Morocco

Numerical Investigation of Natural Convection Heat Transfer Using $\text{TiO}_2/\text{Al}_2\text{O}_3$ -Water Nanofluids

Recently, nanofluids have been used as an alternative in several industries to improve the heat transfer process. This paper focuses on the numerical modeling of the performance of the natural convection process through $\text{TiO}_2/\text{Al}_2\text{O}_3$ -water nanofluids in a square cavity containing a heated block. The lattice Boltzmann method is used in this study to present the nanofluid heat transfer enhancement. Results are presented in terms of streamlines, isothermal contours, and Nusselt number profiles. The findings demonstrate that by raising the Rayleigh number and solid nanoparticle concentration, the average Nusselt number increases, and they reveal that the heated block enormously affects the flow structure and heat transfer. It is also demonstrated that the type of nanoparticles significantly impacts the natural convection heat transfer.

Keywords: Natural convection, Nanofluid, Lattice Boltzmann Method, Heat Transfer, Rayleigh Number.

1. INTRODUCTION

In the last century, the enhancement of heat transfer has become the most requested and interesting topic for engineers and scientists in many areas. Rapid technological advancement proves that using nanofluids is one of the methods to enhance heat transfer due to their specific characteristics and properties compared to pure fluids [1–3]. Abed et al. [4] investigated heat transfer within a trapezoidal enclosure containing Ag-water nanofluid by using the finite element technique. They concluded that the positive effect of nanoparticles is due to the nanofluid's physical properties, like thermal conductivity, viscosity, and heat capacity. Madhu et al. [5] experimentally investigated the effect of nanoparticle volume fraction with CuO, Al_2O_3 , and TiO_2 on conventional solar. They concluded that heat transfer using Al_2O_3 nanoparticles is improved compared with the use of TiO_2 and CuO ones. Also, they demonstrated that the daily energy efficiency increases with an increase in the concentration of nanoparticles in nanofluid due to its thermal conductivity, viscosity, and, consequently, the heat transfer coefficient. Toghraie et al. investigated numerically the dynamic viscosity of Ag/EG nanofluid for different temperatures and volume fraction values of nanoparticles. They found that the performance of mini-channel heat sinks could be improved by using nanofluids to maintain the proper temperature range for electronic components. Nanofluids for heat transfer enhancement are widely used in many applications, like chemical processes, heating,

cooling, and transport. For this reason, various studies have shown that heat transfer can be significantly improved depending on the type and variety of nanoparticles. Chen et al. [6] experimentally investigated, by using the Al_2O_3 and Graphene nanoparticles, the mixed convective heat transfer in the rectangular channel filled with nanofluid submitted to an electrical field force. They revealed that the heat transfer is enhanced with increasing solid nanoparticle concentration. Ma et al. [7, 8] simulated, by employing the TiO_2 and Al_2O_3 nanoparticles, the nanofluid natural and forced convection using lattice Boltzmann method. They found that the heat transfer can be improved by rising nanoparticle concentration. Also, they found that Al_2O_3 has more heat transfer enhancement effect than TiO_2 for the range $0 \leq \phi \leq 5\%$. However, some studies have shown the opposite influence of solid nanoparticle fraction on heat transfer. Li and Peterson [9] experimentally studied the natural convection of Al_2O_3 /Distilled-water nanofluid. The findings demonstrate that the rising of solid nanoparticle concentration decreases the nanofluid natural convective heat transfer. Similarly, Hu et al. [10] experimentally and numerically investigated the natural convection in an enclosure filled with Al_2O_3 -Water nanofluid, where they demonstrated that, for different nanoparticle volume fractions $\phi = 0.25, 0.5$ and 0.77% , the heat transfer becomes progressively worse as the solid nanoparticles concentration ϕ increases. Neves et al. [11] numerically investigated the performance of two nanofluids ($\text{Al}_2\text{O}_3/\text{TiO}_2$ -water) in forced convection heat transfer in a flat tube of an automobile radiator. They found that using nanofluids in the radiator of automobiles can be advantageous to improve radiator performance because the nanofluids can enhance the processes related to heat transfer and, as a result, the engine performance.

Received: September 2023, Accepted: January 2024

Correspondence to: PhD student Younes Oulahou
Faculty of Sciences, University of Moulay
Ismail, Meknes, Morocco

E-mail: younes.oulahou@edu.umi.ac.ma

doi: 10.5937/fme2401157O

© Faculty of Mechanical Engineering, Belgrade. All rights reserved

FME Transactions (2024) 52, 157-172 157

Natural convection has gained considerable attention, especially in the industry. Dong et al. [12] simulated a natural convection around the dome in the passive containment air-cooling system. Wongchadukul et al. [13] illustrated the natural convection effects in porous tissue in radiofrequency cardiac ablation (RFCA). They comprehensively explained the important natural convection influence on temperatures and blood flow during an RFCA treatment. Also, Liu et al. [14] discussed numerically the forced, natural, and mixed convective heat transfer characteristics of super-critical n-decane in a tube in laminar flow. They found that heat transfer is continuously improved for natural convection with the rise of heat flux. The natural convection phenomena have been examined in the nuclear field, where they are studied by Li et al. [15] in hydrothermal reactors. To save energy transfer, they investigate the natural convection of water around the pseudocritical point in a side-wall heated cylinder, which corresponds to a simplified model of an enclosed hydrothermal reactor. Habtay et al. [16] predicted the outlet temperature of the indirect solar dryer chimney. They found that replacing the normal chimney with a heated chimney can significantly reduce heat loss and increase the chimney's efficiency.

The main models for simulating and modeling the nanofluid flows are the single-phase and two-phase models [17, 18]. In the first one, the pure fluid and solid nanoparticles are assumed to be homogeneous fluids [19]. Saha and Paul [20] investigated the characteristics of nanofluid flow and heat transfer in a pipe by using a single-phase approach. Also, Dero et al. [21] studied the stability analysis of nanofluids with viscous dissipation impact over expanding and narrowing surfaces using a single-phase model. In the two-phase model, nanofluids consist of base fluid and nanoparticles as separate parts, forming a non-homogenous mixture [22]. Akbari et al. [23] presented nanofluid laminar flow and heat transfer by using a two-phase model in the curved micro-mixers. Almitani et al. [24] studied the geometric shape effect of the symmetrical twisted turbulator on the parabolic solar collector behavior using a hybrid nanofluid by adopting a two-phase approach.

As we mentioned, nanofluids have several uses in engineering and industry applications. For complex geometries, real flows are governed by a set of non-linear equations [25, 26]. Therefore, numerical approaches have been used to find suitable and acceptable solutions, like macroscopic methods (finite volume (FVM), finite difference (FDM), and finite element (FEM) methods) and mesoscopic method (Lattice Boltzmann (LBM)). Recently, the LBM has become a powerful and useful technique because of its straightforward mathematical algorithm to solve flow problems in complex geometries numerically. Ebrahimi [27] conducted a numerical nanofluid mixed convection in a trapezoidal-shaped sinusoidal cavity by adopting LBM. Hssikou et al. [28] and Elguennouni et al. [29] studied using the LBM for heat transfer of a gas in a square enclosure. Also, Baliti et al. [30] simulated by the Multi-relaxation time lattice Boltzmann method, natural convection in a triangular enclosure. Asha et al. [31] conducted a magnetic field impact on heat transfer in a C-shaped enclosure using MRT-LBM. Moreover, the

LBM could simulate the 3D problems. Li et al. [32] and Chen et al. [33] investigated a 3D simulation of condensation enhancement using LBM.

The objective of this work, with a single-phase model, is to investigate the natural convective heat transfer of a $\text{TiO}_2/\text{Al}_2\text{O}_3$ -water Newtonian nanofluid inside a square cavity containing a heated obstacle with different forms. Natural convection in square cavities is of interest in a variety of applications to control fluid flow stability and heat transfer performance as chemical, electronics, and microfluidics processes. The current work focuses on the study of the flow, isotherms patterns, and Nusselt number variation to evaluate the nanoparticle's concentration and heated obstacle effect. In addition, in the last part, we compared the effect of solid nanoparticle types (Al_2O_3 and TiO_2) on improving heat transfer.

2. PROBLEM STATEMENT

The problem being investigated, in two-dimensional, is convective heat transfer in a square enclosure with cold walls (temperature T_C). We placed an inner heated square block in the enclosure center with a hot temperature T_H (Figure 1). The annulus, which is the space between the square cavity and block, is one of the interesting parameters in this study. The nanofluid is assumed to be incompressible, and the solid nanoparticles and the pure fluid are in thermal equilibrium.

Nanofluid natural convection around a hot obstacle in a square cavity is simulated by adopting the Lattice Boltzmann Method (LBM). We defined two aspect ratios, AR_C and AR_0 . AR_C is linked to the annulus, identified as the ratio of the inner square width w to the outer square's width ($AR_C = \frac{w}{L}$). Meanwhile, we defined $AR_0 = \frac{w}{h}$ as the ratio of the width w of the heated block to its height h .

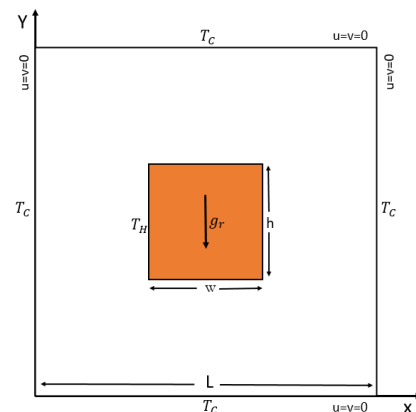


Figure 1. Enclosure geometry.

3. NANOFLUID AND NUMERICAL PROCEDURE

3.1 Nanofluid

From the microscopic viewpoint, the nanofluid performs more distinctly than the pure fluid due to the nanoparticle's presence, so energy transport becomes more effective. Table 1 presents the pure fluid (water) and (Al_2O_3 and TiO_2) nanoparticles' thermo-physical properties.

$$F_y = (\rho\beta)_{nf} g_y (T - T_m), \quad (1a)$$

$$\rho_{nf} = (1 - \varphi)\rho_f + \varphi\rho_{np}, \quad (1b)$$

$$(\rho c_p)_{nf} = (1 - \varphi)(\rho c_p)_f + \varphi(\rho c_p)_{np}, \quad (1c)$$

$$(\rho\beta)_{nf} = (1 - \varphi)(\rho\beta)_f + \varphi(\rho\beta)_{np}, \quad (1d)$$

where φ stands for the nanoparticles volume proportion, ρ is the density; c_p represents the specific heat capacity at constant pressure, β is the thermal expansion coefficient, T_m is the mean temperature $T_m = \frac{T_H + T_C}{2}$, for which subscripts nf , f , and np refer to nanofluid, pure fluid, and nanoparticles, respectively.

Table 1. Thermophysical characteristics of pure fluid and suspended solid nanoparticles.

Physical characteristics	Water	Al ₂ O ₃	TiO ₂
ρ (kg/m ³)	997.1	3970	4250
C_p (J/kg K)	4179	765	686.2
K (W/mK)	0.613	40	8.9538
$\beta \times 10^{-5}$ (K ⁻¹)	21	0.85	0.9
μ (kg/ms)	1.003×10^{-3}	-	-

The nanofluid effective dynamic viscosity μ_{nf} and the effective thermal conductivity k_{nf} models used in this research are provided by Brinkman [34] (2a) and Maxwell [35] (2b) models, respectively:

$$\mu_{nf} = \mu_f \left(\frac{1}{(1 - \varphi)^{2.5}} \right), \quad (2a)$$

$$k_{nf} = k_f \left(\frac{\kappa_{np} + 2\kappa_f - 2\varphi(\kappa_f - \kappa_{np})}{\kappa_{np} + 2\kappa_f - \varphi(\kappa_f - \kappa_{np})} \right). \quad (2b)$$

3.2 Numerical procedure

The present LBM model employs two distribution functions to calculate the flow density (f) and the temperature (g) fields in order to investigate the fluid and heat transport. The governing equations of these functions are given, respectively, by:

$$f_i(x + c_i \Delta t, t + \Delta t) - f_i(x, t) = -\frac{1}{\tau_f} (f_i(x, t) - f_i^{eq}(x, t)) + \Delta F_i, \quad (3a)$$

$$g_i(x + c_i \Delta t, t + \Delta t) - g_i(x, t) = -\frac{1}{\tau_g} (g_i(x, t) - g_i^{eq}(x, t)), \quad (3b)$$

where τ_f (τ_g) is the relaxation time for the flow (temperature) field, Δt represents the lattice time step ($\Delta t = 1$), and c_i is the discrete particle velocity vector in the i -direction.

$$c_i = \begin{cases} (0, 0), i = 0 \\ c \left(\cos \left[(i-1) \frac{\pi}{2} \right], \sin \left[(i-1) \frac{\pi}{2} \right] \right), i = 1-4 \\ \sqrt{2}c \left(\cos \left[(i-1) \frac{\pi}{2} \right], \sin \left[(i-1) \frac{\pi}{2} \right] \right), i = 5-8 \end{cases} \quad (4)$$

The term $f_i^{eq}(g_i^{eq})$ is the flow's (temperature) local equilibrium distribution function in second (first) order, given as:

$$f_i^{eq}(x, t) = \omega_i \rho \left(1 + \frac{3(c_i \cdot u)}{c^2} + \frac{9(c_i \cdot u)^2}{2c^4} - \frac{3u^2}{2c^2} \right), \quad (5a)$$

$$g_i^{eq}(x, t) = \omega_i T \left(1 + \frac{3(c_i \cdot u)}{c^2} \right), \quad (5b)$$

where the quantities ρ , u , and T indicate macroscopic density, velocity, and temperature, respectively. ω_i are the weight factors for both flow density and temperature, as follows:

$$\omega_i = \begin{cases} 4/9, i = 0 \\ 1/9, i = 1-4 \\ 1/36, i = 5-8 \end{cases} \quad (6)$$

Figure 2 illustrates the D₂Q₉ model for both flow and temperature.

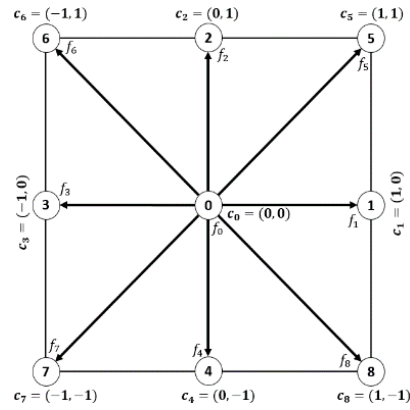


Figure 2. The discrete velocities set of the D₂Q₉ model.

The relaxation times τ_f and τ_g are linked to the kinematic viscosity ν and thermal diffusivity α , respectively, by:

$$\nu = \left[\tau_f - \frac{1}{2} \right] c_s^2 \Delta t, \quad (7a)$$

$$\alpha = \left[\tau_g - \frac{1}{2} \right] c_s^2 \Delta t, \quad (7b)$$

where c_s is the sound speed.

By setting Mach number (Ma), Rayleigh number (Ra), and Prandtl number (Pr), the kinematic viscosity ν is obtained by:

$$\nu = c_s Ma N \sqrt{Pr / Ra}, \quad (8)$$

where N denotes the lattice number in the y -direction. Prandtl (Pr) and Rayleigh (Ra) numbers are given by:

$$Pr = \frac{\nu}{\alpha}, \quad (9a)$$

$$Ra = \frac{\beta g_y N^3 (T_H - T_C)}{\alpha \nu}. \quad (9b)$$

We defined the characteristic flow velocity v_{scale} as:

$$v_{\text{scale}} = \frac{1}{L} \sqrt{Ra \cdot \nu \cdot \alpha} \quad (10)$$

The external force term F_i of this problem of natural convection, which is applied in the collision step, as shown in (3a), is provided by:

$$\mathbf{F}_i = \frac{\omega_i}{c_s^2} F_y \mathbf{c}_i, \quad (11)$$

where $F_y = \rho \cdot g_r \cdot \beta \cdot \Delta T$ is the buoyancy force term, g_r is the vertical component of the gravitational vector, and ΔT is defined as $\Delta T = T - T_m$ with $T_u = \frac{T_H + T_C}{2}$

$$\rho = \sum_{i=0}^8 f_i, \quad (12a)$$

$$\rho \mathbf{u} = \sum_{i=0}^8 f_i \mathbf{c}_i, \quad (12b)$$

$$T = \sum_{i=0}^8 g_i. \quad (12c)$$

The Nusselt number is used to quantify heat transfer improvement, and a rise in the Nusselt number signifies enhanced heat transfer.

Along the hot right wall, the local Nusselt number Nu and its average value Nu_{avg} are calculated respectively, as follows:

$$Nu = -\frac{\kappa_{nf}}{\kappa_f} \frac{L}{T_H - T_C} \left(\frac{\partial T}{\partial x} \right)_{x=0}, \quad (13a)$$

$$Nu_{\text{avg}} = \frac{1}{L} \int_0^L Nu \cdot dy, \quad (13b)$$

where T is the normalized temperature.

3.3 Boundary conditions

Boundary conditions play a crucial role in micro-geometries simulation.

For the flow field, the standard bounce-back boundary condition [36,37] was implemented in obstacle boundaries and walls of the cavity. For example, at the right wall of the cavity and solid obstacle wall, the unknowns' distributions are, respectively:

$$\begin{cases} f_1 = f_3 \\ f_5 = f_7 \\ f_8 = f_6 \end{cases}, \quad (14a)$$

$$\begin{cases} f_3 = f_1 \\ f_7 = f_5 \\ f_6 = f_8 \end{cases}. \quad (14b)$$

For the temperature field, the boundary conditions used in this study are conducted by Mohamad [38]. On the hot bottom wall of the obstacle, the unknowns' distributions are g_4 , g_7 , and g_8 , which are evaluated as:

$$\begin{cases} g_4 = T_H (\omega_4 + \omega_2) - g_2 \\ g_7 = T_H (\omega_7 + \omega_5) - g_5 \\ g_8 = T_H (\omega_8 + \omega_6) - g_6 \end{cases}. \quad (15a)$$

On the cold bottom wall of the cavity, the unknowns' distributions are g_2 , g_5 , and g_6 , which are calculated as:

$$\begin{cases} g_2 = T_H (\omega_2 + \omega_4) - g_4 \\ g_5 = T_H (\omega_5 + \omega_7) - g_7 \\ g_6 = T_H (\omega_6 + \omega_8) - g_8 \end{cases}. \quad (15b)$$

4. RESULTS AND DISCUSSION

4.1 Grid stability

In this part, we calculate the Nu_{avg} for various grid sizes, from 60×60 to 150×150 . Table 2 below shows that Nu_{avg} stabilizes from 140×140 . Also, it is observed from Figure 3 that the v -velocity profiles maximize from the grid size 140×140 . Therefore, the current numerical simulations choose the grid size of 140×140 .

Table 2. Grid independence test for TiO_2 , $\phi = 4\%$, and $\text{AR}_c = 0.25$.

Grid size	Nu_{avg}
60×60	0.8925
80×80	0.9688
100×100	0.9691
120×120	1.0150
140×140	1.0116
150×150	1.0101

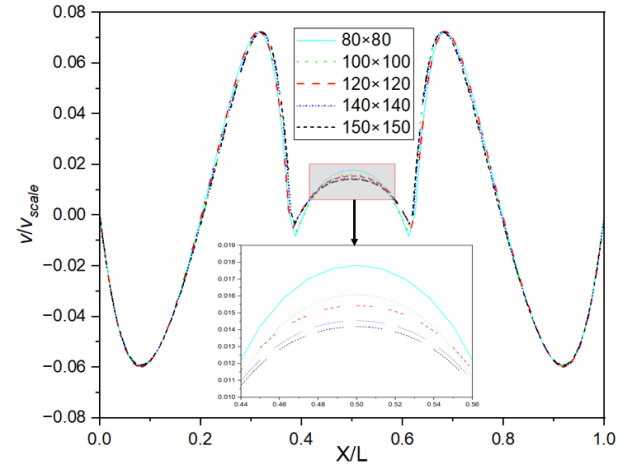


Figure 3. v -velocity component along the horizontal $\text{ARC} = 0.25$ centerline for different uniform grids, $\phi = 4\%$, $\text{ARC} = 0.2$ and $Ra = 10^5$.

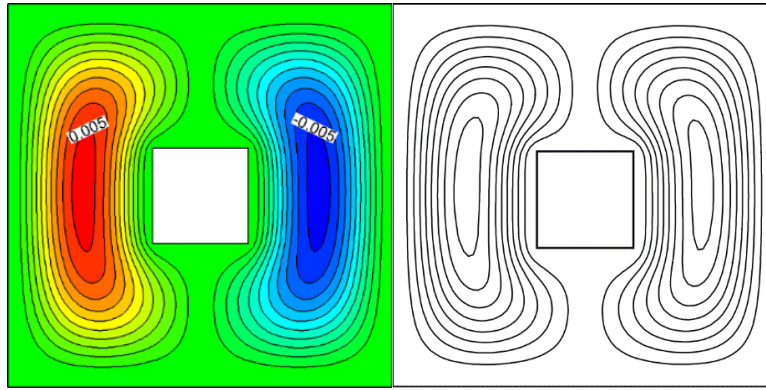
To check the validity of the obtained results, we compared them with those of Arefmanesh et al. [39], in terms of streamlining and isotherm profiles (figures 4 and 5) for TiO_2 -water nanofluid. As seen in these comparisons, our findings are in agreement with those of Arefmanesh et al. [39].

We note that negative flow function values in all streamline profiles describe counterclockwise circulation inside the cavity.

In order to validate our simulation, we also compare our results (streamlines and isotherms profiles) with the experimental and numerical results of natural convection in a cavity occupied with air ($Pr = 0.71$) [40].

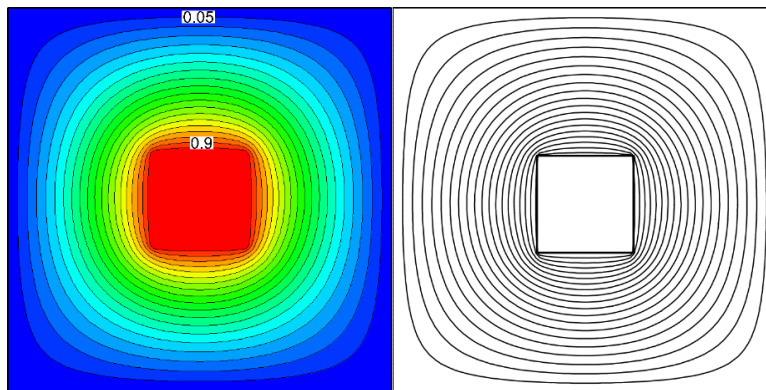
The heat source (temperature T_H) length is $d = \frac{2}{5}L$, and its center is located at the position $x_d = 0.3H$ on the bottom side of the enclosure.

$$|\psi_{max}| = 0.0051401$$



(a) $\phi = 4\%$, present results.

(b) $\phi = 4\%$, Arefmanesh et al.[39].

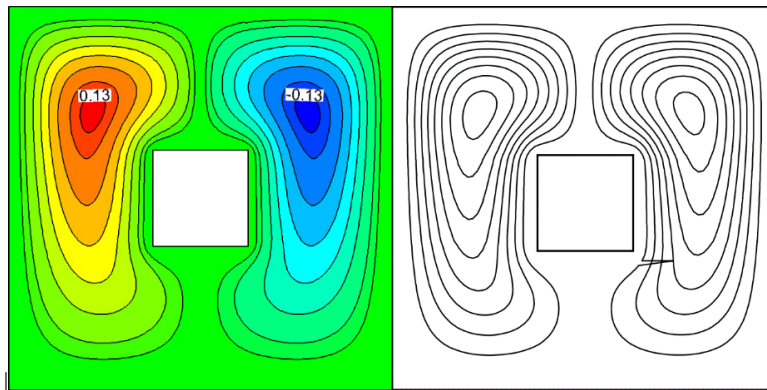


(c) $\phi = 4\%$, present results.

(d) $\phi = 4\%$, Arefmanesh et al.[39].

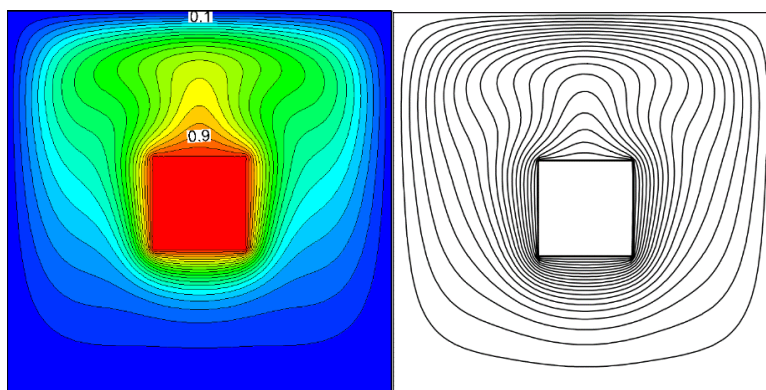
Figure 4. Streamlines (a and b) and isotherms (c and d) for $Ra = 10^3$.

$$|\psi_{max}| = 0.1328418$$



(e) $\phi = 4\%$, present results.

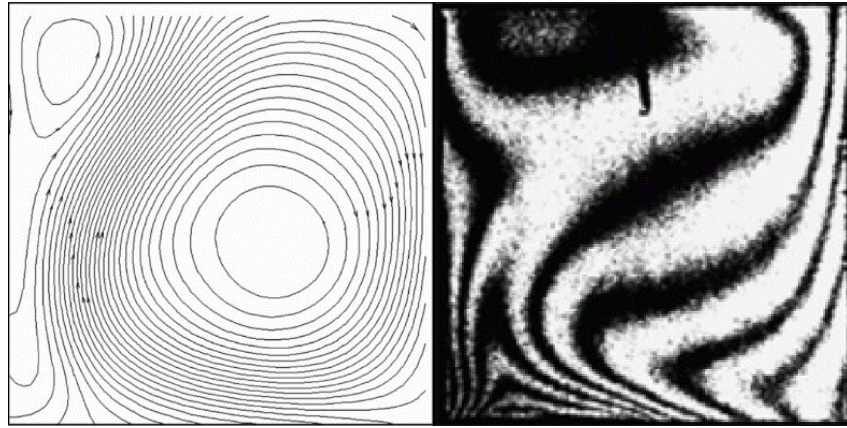
(f) $\phi = 4\%$, Arefmanesh et al.[39].



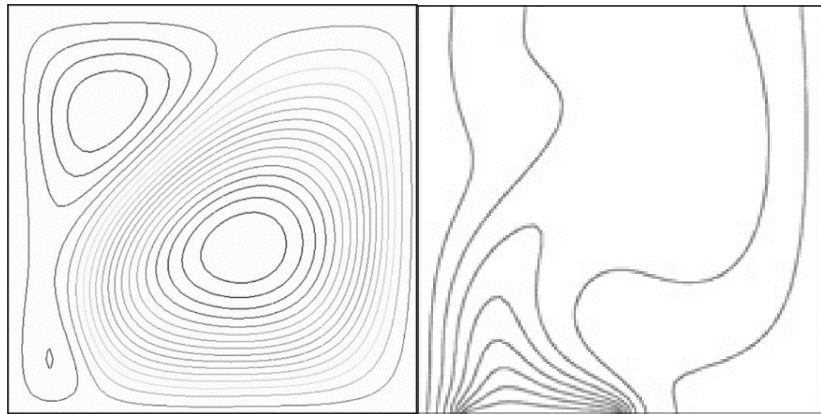
(g) $\phi = 4\%$, present results.

(h) $\phi = 4\%$, Arefmanesh et al.[39].

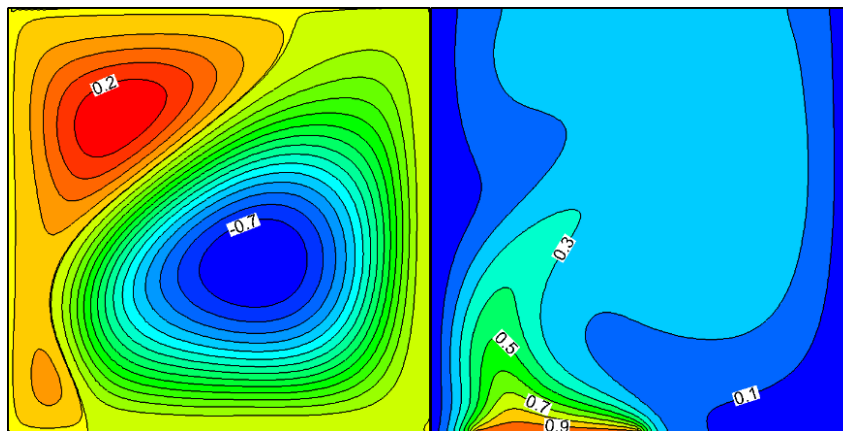
Figure 5. Streamlines (e and f) and isotherms (g and h) for $Ra = 10^5$.



(a) Experimental data of Corvaro et Paroncini [40]. (b) Experimental data of Corvaro et Paroncini [40].



(c) Numerical data of Corvaro et Paroncini [40]. (d) Numerical data of Corvaro et Paroncini [40].



(e) Present results.

(f) Present results.

Figure 6. Streamlines (a, c, and e) and isotherms (b, d, and f) for $Ra = 1.26 \times 10^5$ in the case of air.

Both vertical walls are maintained at a cold temperature (T_C), while the top wall is adiabatic. This examination shows that the experimental and numerical data of Corvaro and Paroncini [40] and our numerical findings are in agreement (figure 5).

4.2 Effect of nanoparticle concentration

In this part, we discussed the effect of Al_2O_3 nanoparticles concentration $0 \leq \phi \leq 16\%$ on the streamlines and isotherm profiles for Rayleigh number value 105 and $ARC = 0.25$ (figure 7).

Figure 7(a-c) illustrates the streamline profiles, which demonstrate that the eddies of the two circula-

tions are close to each other within the top portion of the annulus due to high Ra . Also, with an increase in nanoparticle concentration ϕ , the shape of two vortices increases and occupies more space. Note that the two vortices are counter-rotating, which means that they have opposite directions of rotation. For the isotherm profiles, with augmentation of nanoparticles concentration ϕ , as a result of the rise of effective thermal conductivity α_{nf} , the hot isolines expand and run away from the top of the inner square, while the cold ones move upward to the top surface of the outer square. For the bottom side, the nanofluids shrink to the inner body and come far and away from the bottom surface under the impact of the buoyancy force (Figure 7(d-f)).

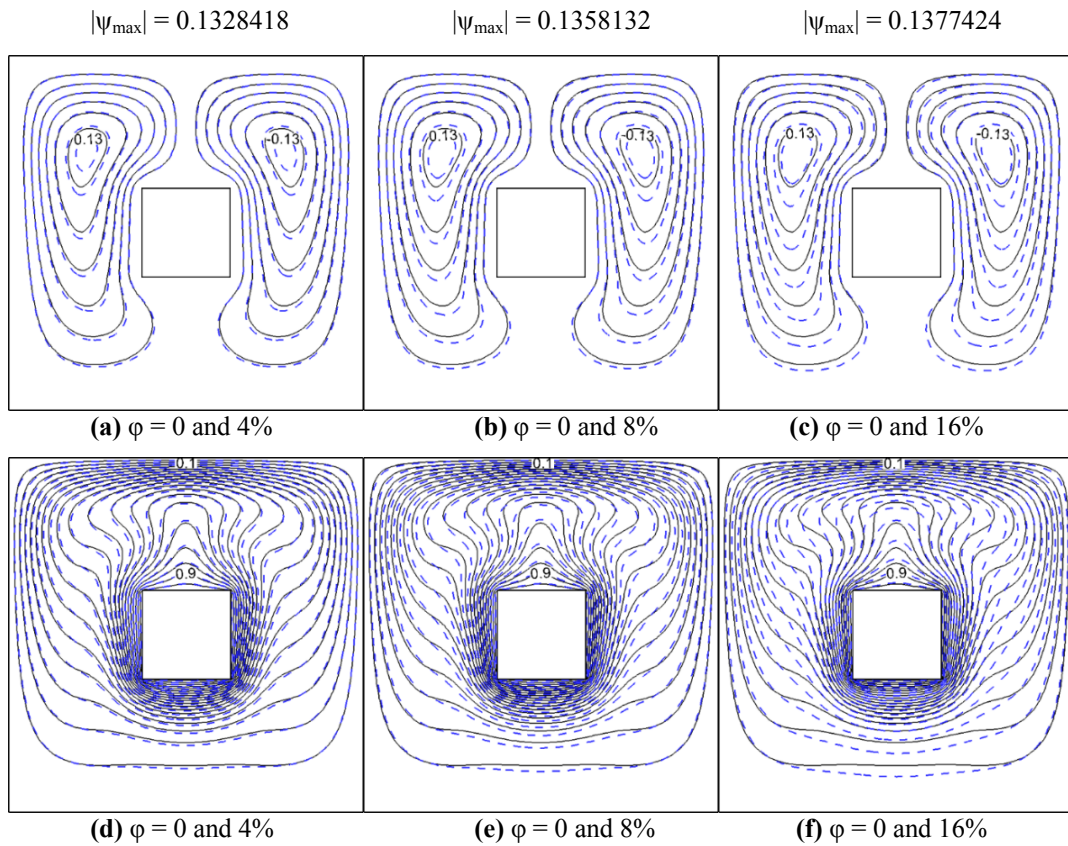


Figure 7. Streamlines (a-c) and isotherms (d-f) for $Ra = 10^5$ with (-) $\phi = 0\%$ and (---) $\phi = 4\%$ $\phi = 8\%$ and $\phi = 16\%$ for $AR_c = 0.25$.

4.3 Effect of Rayleigh number

The effect of Rayleigh number (Ra) for a particular nanoparticle concentration ϕ and aspect ratio of annulus $AR_c = 0.25$ in terms of streamlines and isotherms is

investigated (figure 8). Figure 8(a-c) demonstrates that with the increasing of Ra , the absolute value of the maximum flow function $|\Psi_{max}|$ increases (from $|\Psi_{max}| = 0.0050667$ for $Ra = 10^3$.

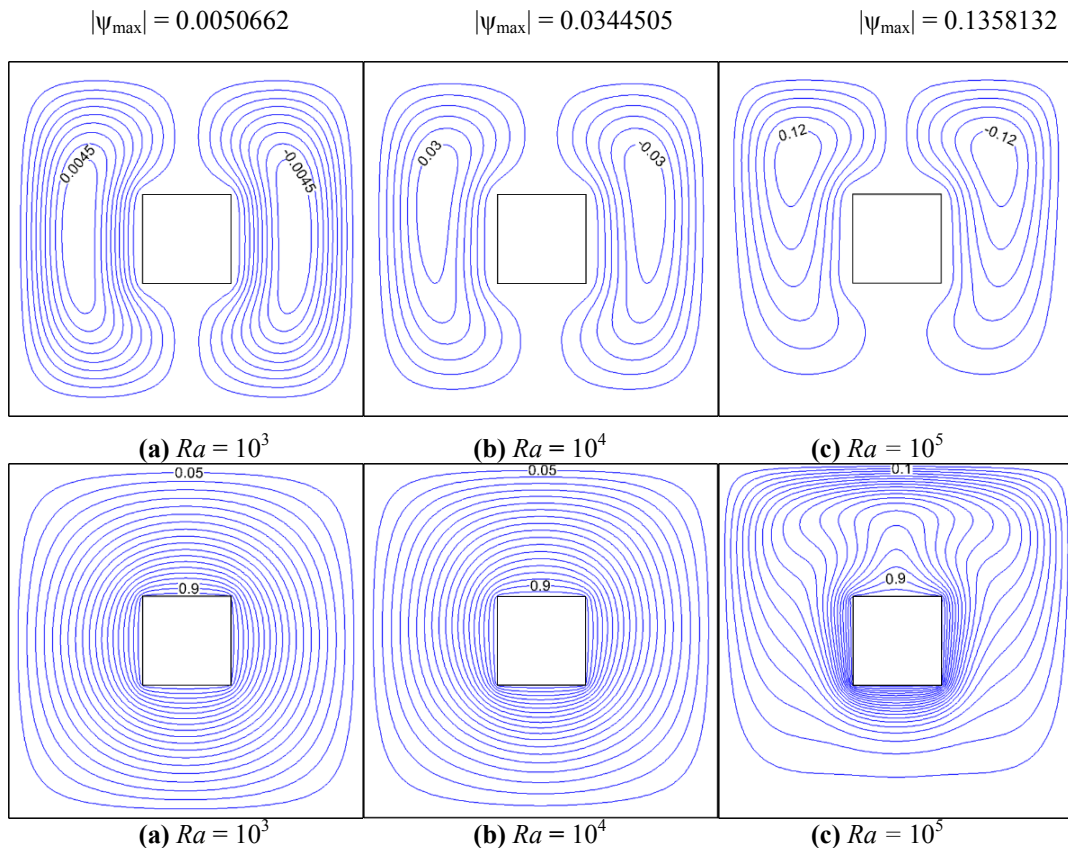


Figure 8. Streamlines (a-c) and isotherms (d-f) for $\phi=8\%$, $AR_c = 0.25$, and different Ra values.

To $|\psi_{\max}| = 0.1358132$ for $Ra = 10^5$, which means that the stream function expands and takes more space, so the convection begins, and then the heat transfer enhances in the nanofluid. Also, the two counter-rotating eddies come close to each other on the top portion of the enclosure for $Ra = 10^5$ more than for $Ra = 10^3$.

As shown in Figure 8(d-f), by raising the Rayleigh number Ra , as a result of buoyancy forces, the isolines alter their process, go up and down, and gather at the top surface.

4.4 Effect of heated block size

To evaluate the effect of heated block size, three values of $AR_C = 0.25, 0.5,$ and 0.75 , for a particular nanoparticle's concentration $\phi = 8\%$ and Rayleigh number $Ra = 10^5$, are considered. The findings show that the aspect ratio of the heater affects the flow structure and heat transfer distribution.

Moreover, they show that as the inner square size increases, the streamlines and isotherms get denser and closer to each other inside the annulus, figure 9.

Figure 9(a-c) illustrates that with the increasing aspect ratio AR_C from 0.25 to 0.75, the circulation of streamlines expands vertically, and new vortices are created. Also, with the rising of AR_C , the absolute value of the maximum flow function decreases; from $|\psi_{\max}| = 0.1358132$ for $AR_C = 0.25$ to 0.0074749 for $AR_C = 0.75$, therefore, the convection process becomes worse due to the narrowing of the annulus.

For isotherm profiles, as shown in figure 9(d-f), with the increase of the aspect ratio AR_C , the temperature gradients get close to cavity walls and accumulate. Also, as the nanofluid is cooled by the boundaries of the outer square and heated by the block walls, the increasing aspect ratio AR_C made the hot isotherms occupy more space, which means the conduction process enhances the heat transfer.

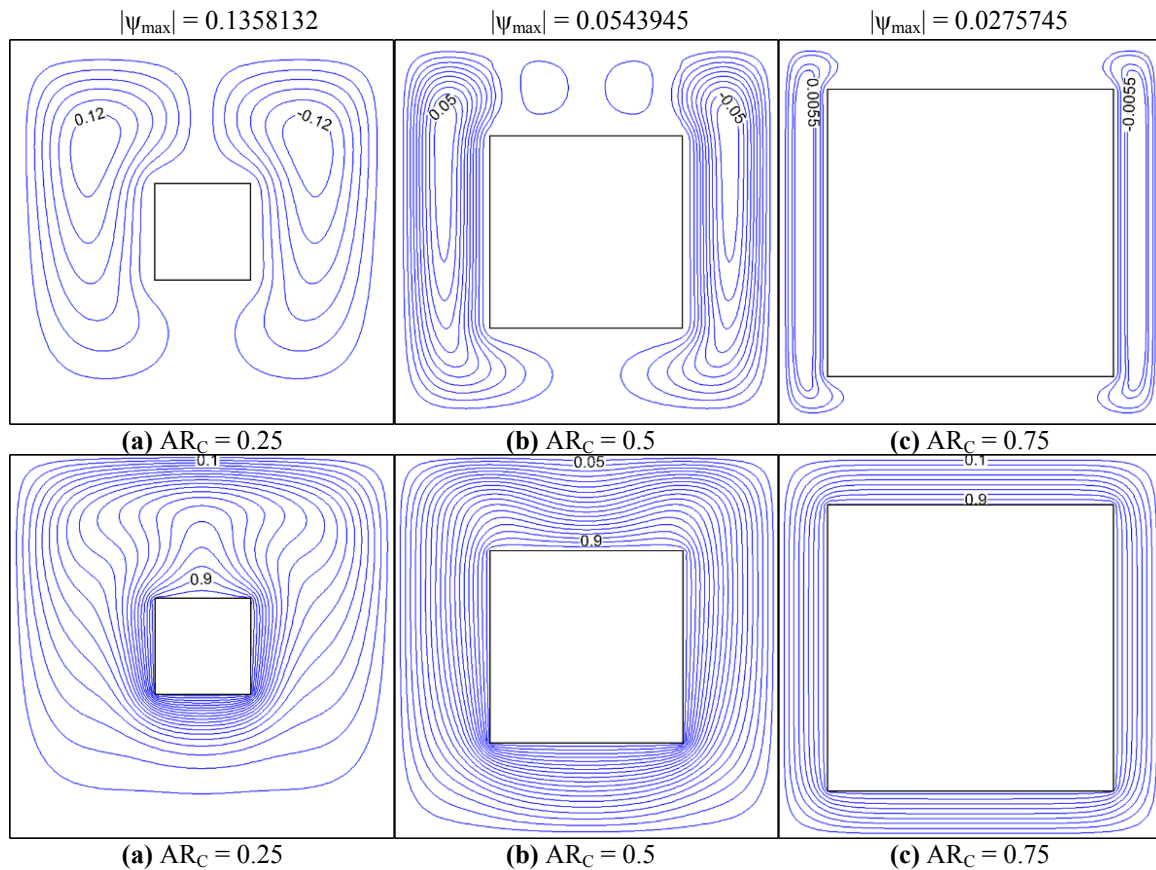


Figure 9. Streamlines (a-c) and isotherms (d-f) for $Ra = 10^5$, $\phi = 8\%$, and different AR_C values.

4.5 Overall heat transfer change

Figure 10(a-c) shows the dependence of the average Nusselt number (Nu_{avg}), calculated along the right surface of the inner square, on the nanoparticle's concentration for several Rayleigh numbers values Ra and different aspect ratio values AR_C . For all nanoparticle fractions ϕ values, the Nu_{avg} increases as Ra and AR_C increase, i.e., heat transfer is enhanced as the Rayleigh number, nanoparticles concentration ϕ , and the aspect ratio AR_C rise. The findings demonstrate that the Nu_{avg} is more sensitive to the highest Rayleigh number for $AR_C = 0.25$. The values of Nu_{avg} for $Ra =$

10^4 move away from those of $Ra = 10^3$ to those of $Ra = 10^5$ as AR_C increases. Moreover, for all Rayleigh numbers and values, the Nu_{avg} rises with the rising of solid nanoparticles concentration ϕ .

Figure 11 illustrates the average Nusselt number Nu_{avg} values for various aspect ratio ones AR_C (0.25, 0.5, and 0.75) and a particular volume fraction of nanoparticles $\phi = 8\%$. The Nu_{avg} for all values of AR_C , increases faster for lower Ra values. At the same time, it increases slowly for higher Ra due to the decrease of dynamic viscosity μ_{nf} .

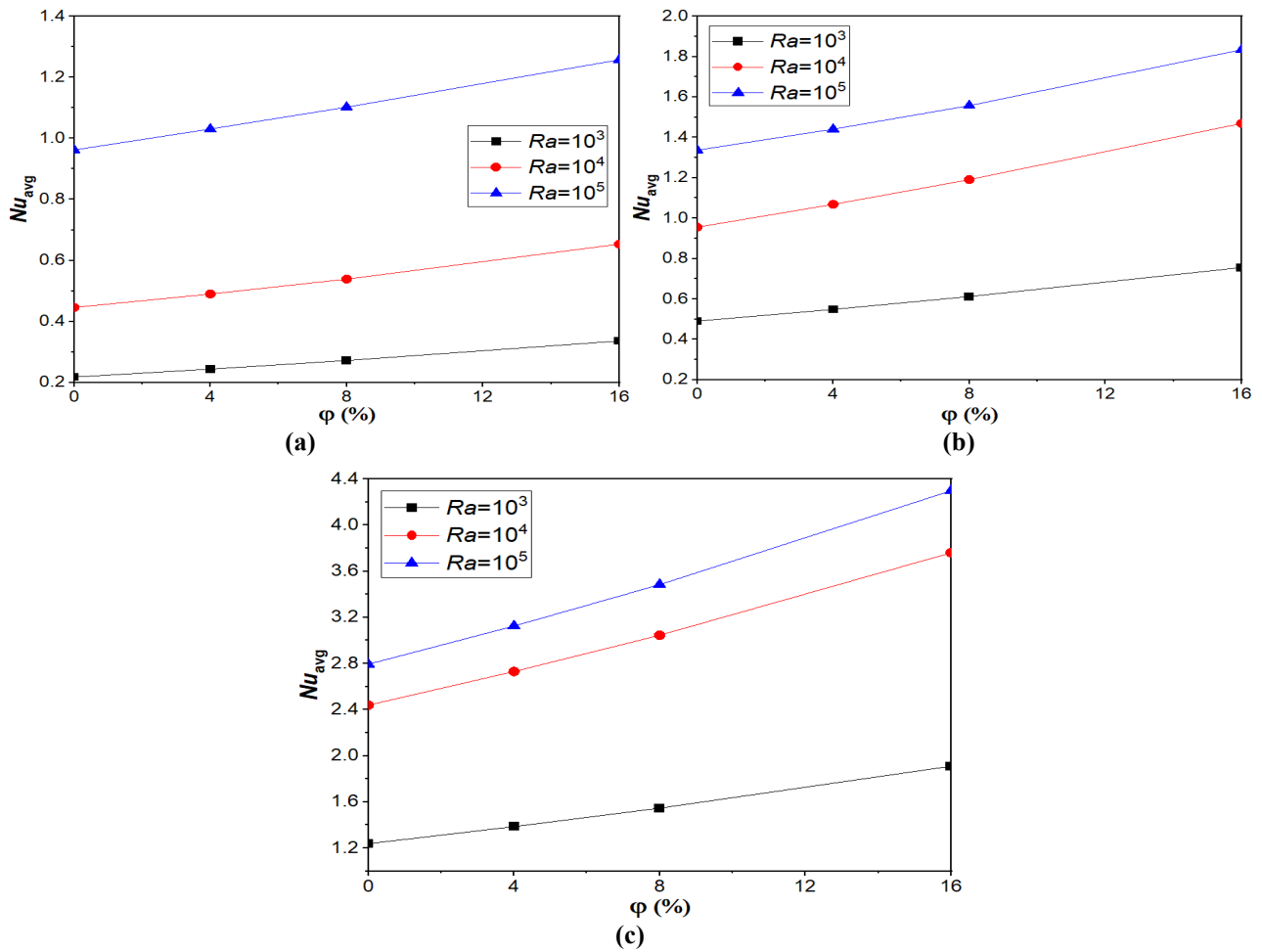


Figure 10. Average Nusselt number variation on the right surface of the inner square, (a) $AR_c = 0.25$, (b) $AR_c = 0.5$, and (c) $AR_c = 0.75$.

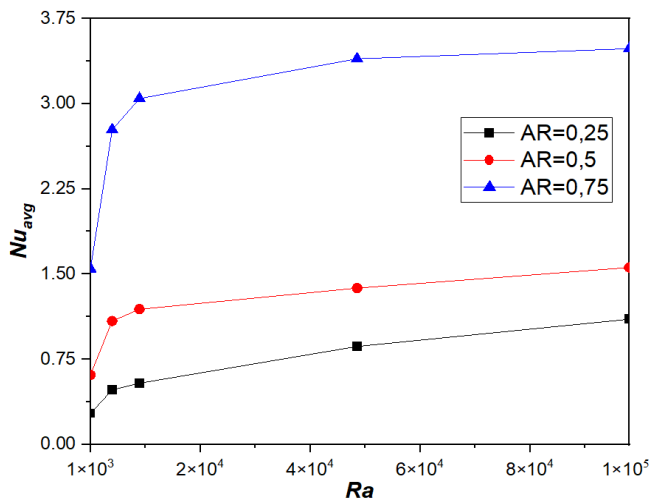


Figure 11. Average Nusselt number variation on the right wall of the inner square for $\phi = 8\%$

4.6 Temperature and v-velocity profiles

Figure 12(a) shows that in the cold parts, on the right and left sides of the obstacle, the nanoparticle concentration ϕ has a slight effect (the zoomed part at the bottom). While, at the hot block, with increasing the nanoparticles concentration ϕ , the normalized temperature distribution increases and gets better due to the nanofluid's increasing density and thermal conductivity and the hot block effect.

Far from the obstacle, Figure 12(b), the temperature profile is almost linear for Rayleigh numbers $Ra = 10^3$ and $Ra = 10^4$ due to the conduction dominance. Meanwhile, for $Ra = 10^5$, the temperature profile is more affected by the increase of Ra due to viscosity decreasing, so the convection process increases, as figure 8 demonstrates.

Figure 12 (c) shows that by increasing the aspect ratio of annulus AR_c , the profile of temperature changes from a curved to a linear shape, which means that the conduction process increases and the convection decreases, as shown in figure 9.

Figure 13 (a) exhibits the vertical velocity component plots along the horizontal line $\frac{y}{L} = 0.5$, for $Ra = 10^5$, $AR_c = 0.25$, and different nanoparticle concentrations ϕ . The results demonstrate that with increasing the nanoparticles concentration ϕ , the maximum magnitude of v-velocity of the nanofluid decreases dramatically due to the increasing nanofluid thermal conductivity.

Figure 13 (b) demonstrates that with a rise of Rayleigh number, for $\phi = 8\%$ and $AR_c = 0.25$, the amplitude of v-velocity increases due to a decrease of viscosity μ , which means the enhancement of heat transfer as demonstrated in Figure 8. An insight in figure 13 (c) shows that with a rise of aspect ratio $AR_c = 0.25$, for $\phi = 8\%$ and $Ra = 10^5$, the fluid velocity rises due to a decrease in nanofluid diffusivity.

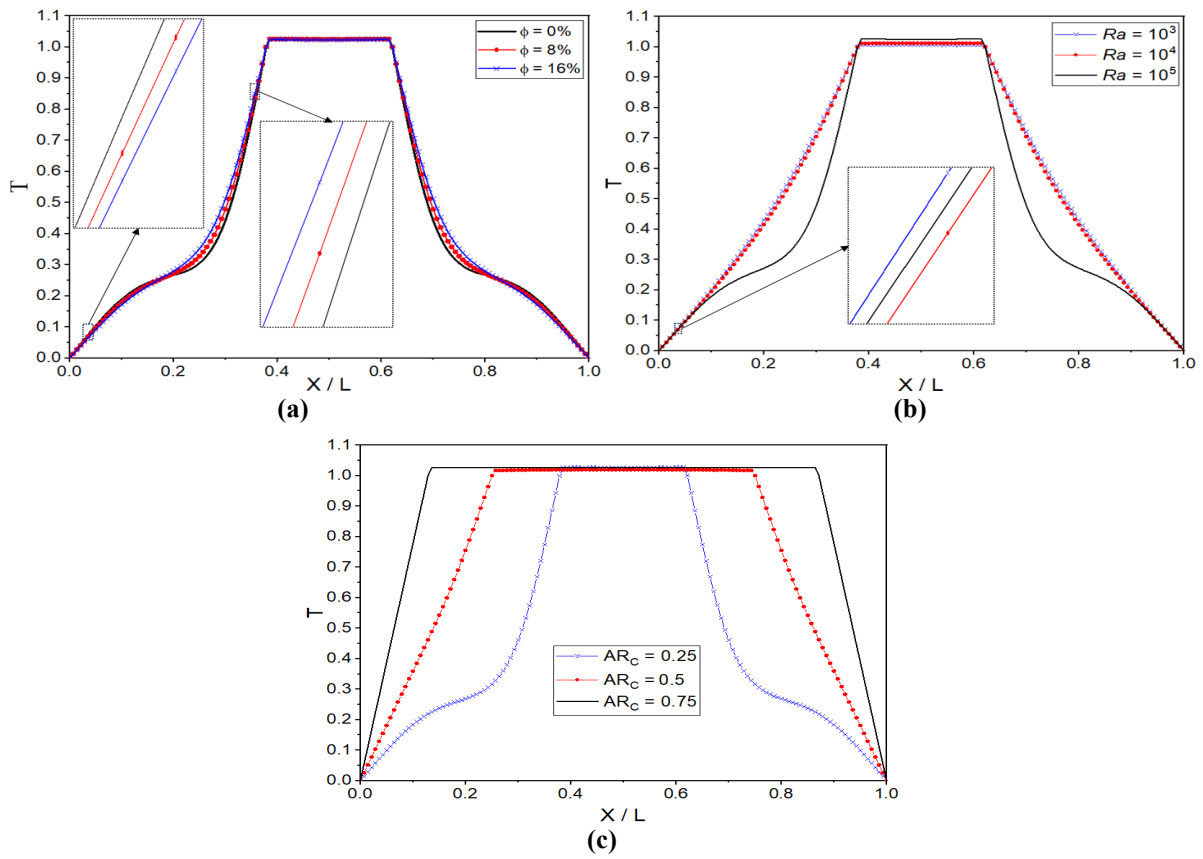


Figure 12. Temperature profiles along the horizontal line $\frac{y}{L} = 0.5$. for (a) $Ra = 10^5$ and $AR_c = 0.25$, (b) $\phi = 8\%$ and $AR_c = 0.25$, and (c) $Ra = 10^5$ and $\phi = 8\%$.

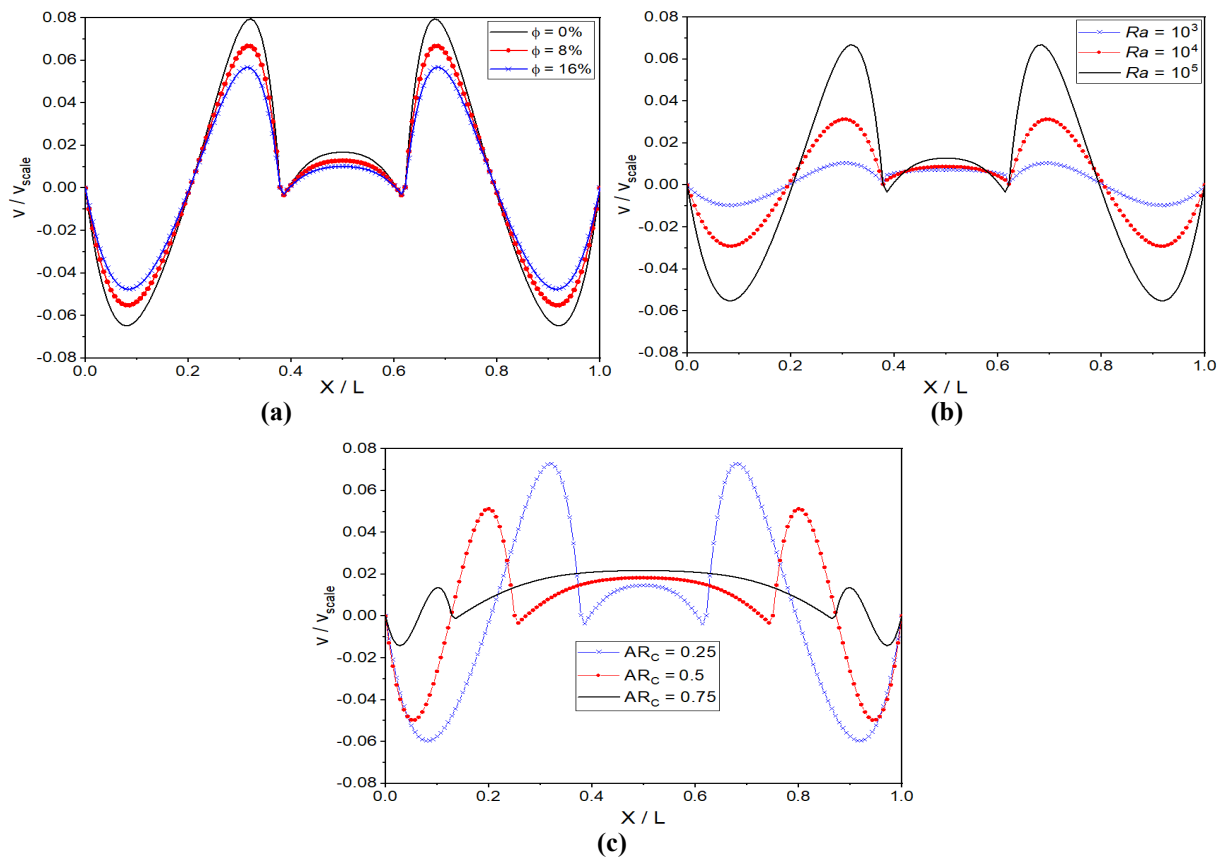


Figure 13. v -velocity profiles along the horizontal line $\frac{y}{L} = 0.5$. for (a) $Ra = 10^5$ and $AR_c = 0.25$, (b) $\phi = 8\%$ and $AR_c = 0.25$, and (c) $Ra = 10^5$ and $\phi = 8\%$.

4.7 Effect of heated block form

To investigate the effect of heat block form, we changed the dimension of the inner heated block $AR_0 = \frac{w}{h}$ from the square form to rectangular one for two values: Rayleigh number Ra (10^3 and 10^5) and nanoparticle concentrations ($\phi = 0\%$ and 8%). Their outcomes are shown in Figure 14s 14 and 15. For $AR_0 = 2$, figure 14 (a) shows the appearance of four eddies instead of two. Moreover, it demonstrates that as the concentration of nanoparticles rises, the vortices become deeper within the cavity as well as the intensity of streamlines decreases ($|\psi_{max}| = 0.09890929$) for $Ra = 10^5$ and $\phi = 8\%$, compared to the inner square obstacle ($|\psi_{max}| = 0.1358132$ (figure 8 (c)), so the natural convection does not enhance. While there is no sensible change in the

isotherms due to the low Rayleigh number value $Ra = 10^3$ (figure 14 (b)). For $Ra = 10^5$ (figure 14(c)), the convection process increases with the increase in nanoparticle concentration. The isolines become expanded beside and around the heated obstacle (figure 14(d)).

Figure 15 (a) shows that the streamlines expand vertically, and the maximum values of flow function decrease slightly ($|\psi_{max}| = 0.0053271$) for $Ra = 10^3$ and $\phi = 0\%$ compared to the inner square obstacle ($|\psi_{max}| = 0.0050662$), figure 8(a), so the natural convection decreases. In addition, for all forms of the heated block, as Rayleigh number Ra and nanoparticle concentrations ϕ increase, $|\psi_{max}|$ increases, and the hot isolines expand, therefore enhancing heat transfer.

Figures 14 and 15 demonstrate that the form of the heated block plays a significant role in controlling natural convection.

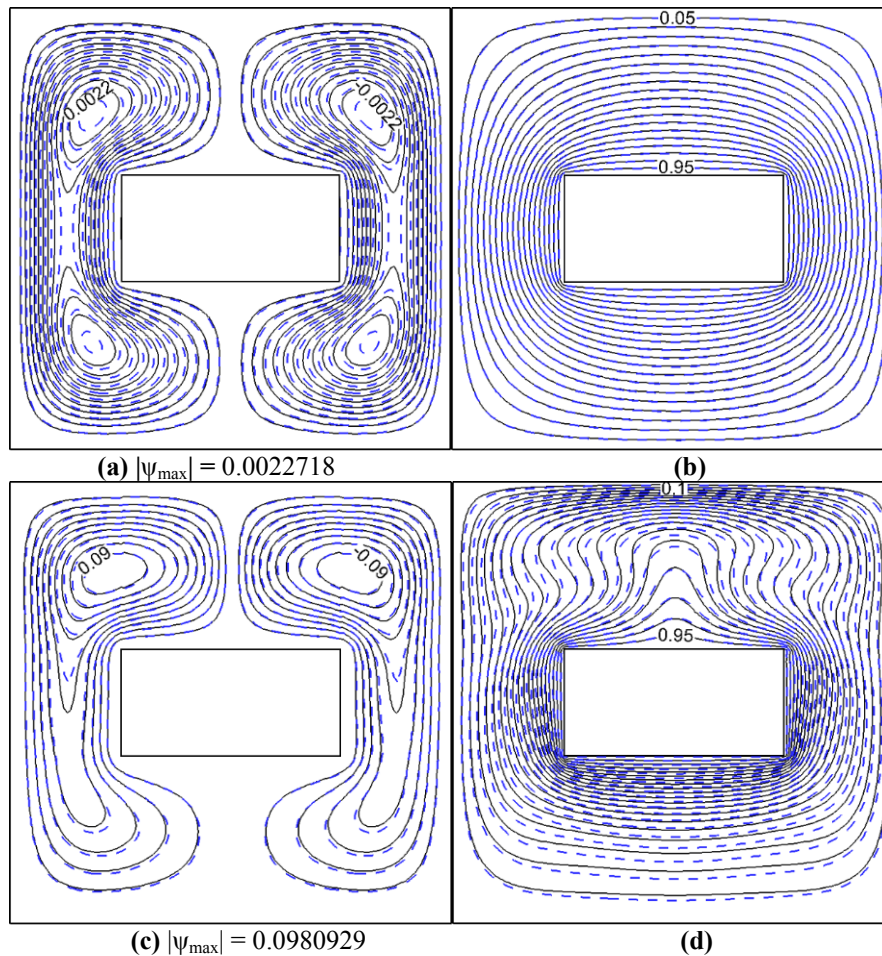


Figure 14. Streamlines (On the left) and isotherms (on the right), (a-b) $Ra = 10^3$ and (c-d) $Ra = 10^5$, for (-) $\phi = 0\%$ and (---) $AR_0 = 2$, $\phi = 8\%$.

The influence of the heated block form on the average Nusselt number Nu_{avg} will be discussed in this part for $Ra = 10^5$ and three values of $AR_0 = 0.5, 1$, and 2 . Figure 16(a-b) demonstrates that the Nu_{avg} , calculated along the right hot wall of the block and on the outer square right wall, for different values of nanoparticles concentration ϕ (0-8%), is higher for the lowest aspect ratio AR_0 . These findings reveal that the heat transfer from a heated wall to a fluid enhances $AR_0 = 0.5$ more than $AR_0 = 1$ and $AR_0 = 2$.

Figure 16(c-d) illustrates the average Nusselt number Nu_{avg} along the block's top layer and outer

square. For the block square, the Nu_{avg} is better for the higher aspect ratio ($AR_0 = 2$) (Figure 16(c)). Meanwhile, for the outer square, the Nu_{avg} is higher for the lowest aspect ratio, $AR_0 = 0.5$ (Figure 16(d)).

From the result, the higher Nusselt number of the block square depends on the interested surface. For the outer square, the highest Nusselt number is for the lowest aspect ratio ($AR_0 = 0.5$) as a result of the effective thermal con-ductivity enhancement, and the hot isolines expand to the surface of the outer square, so the transfer increases and enhances.

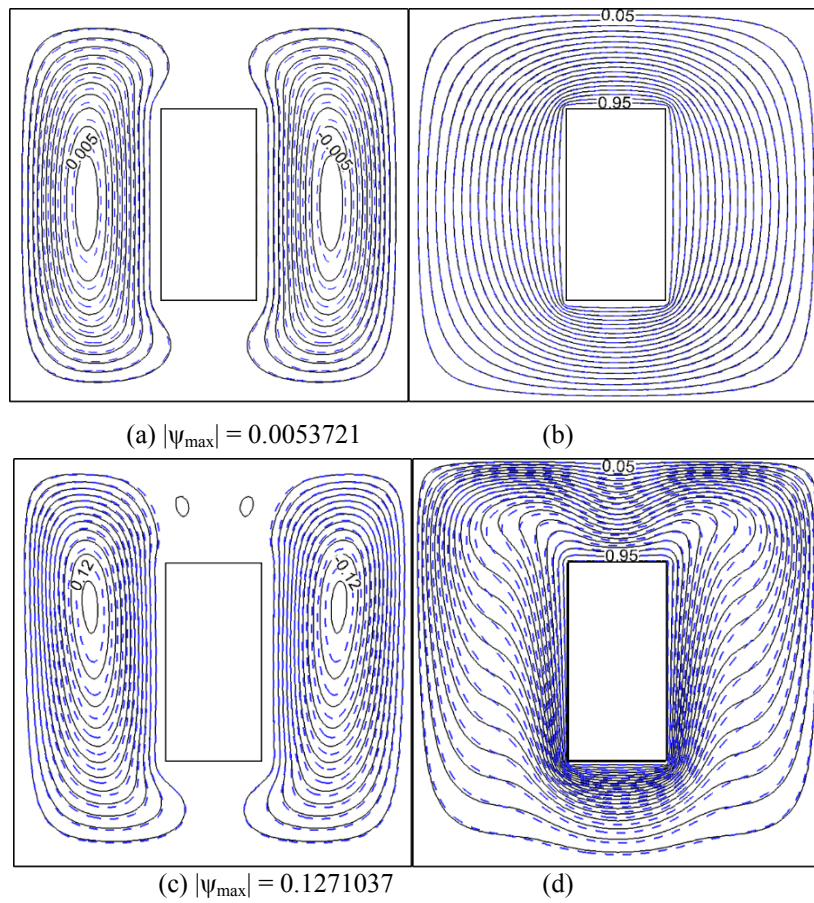


Figure 15. Streamlines(On the left) and isotherms(on the right),(a-b) $Ra = 10^3$ and (c-d) $Ra = 10^5$, for (-) $\phi = 0\%$ and (---) $\phi = 8\%$ $AR_0 = 0.5$.

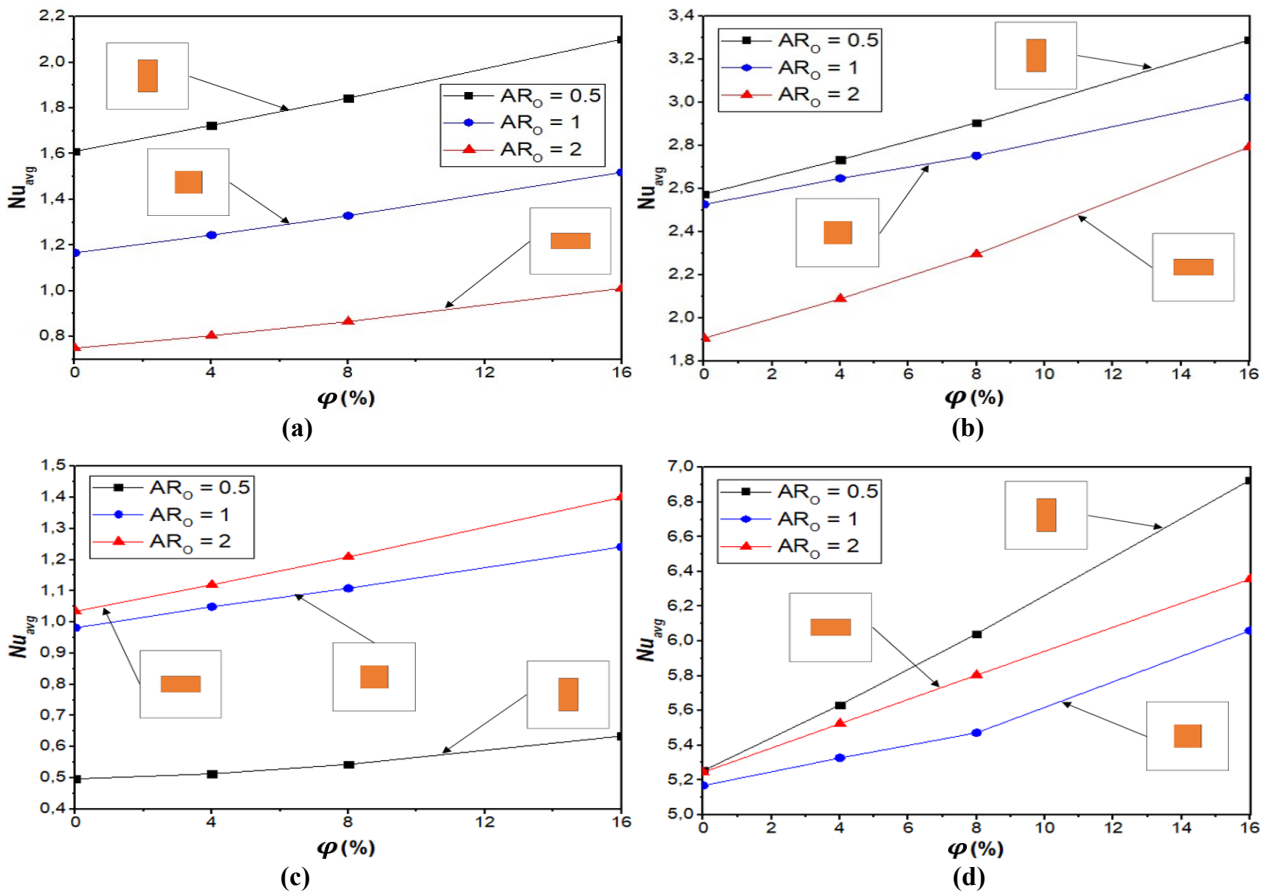


Figure 16. The average Nusselt numbers variation on the right wall (a and b) and on the upper wall (c and d) of heater block (a and c) and outer square (b and d), for $Ra = 10^5$.

4.8 Nanoparticles type

To study the impact of solid nanoparticle type on the heat transfer of nanofluid, the two different nano-particles, Al_2O_3 and TiO_2 , are taken into consideration for $Ra = 10^5$, AR_C , and different volume fractions of nanoparticles ($0 \leq$

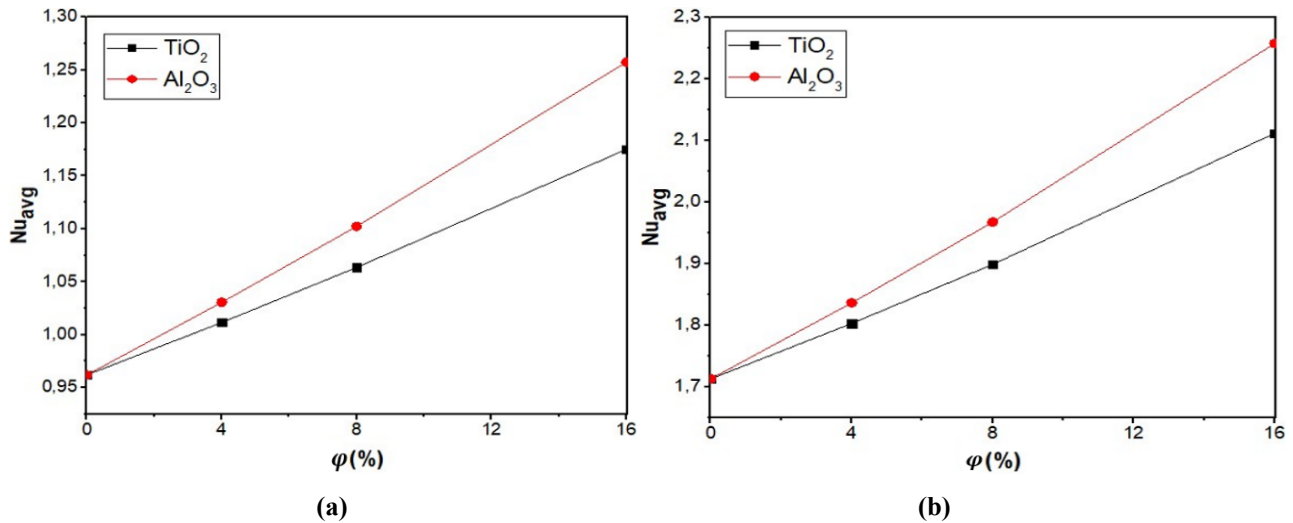


Figure 17. Average Nusselt number variation of two nanoparticle types on the right wall of the heater block (a) and outer square (b) for $Ra = 10^5$ and $AR_0 = 0.25$.

5. CONCLUSION

The present work discussed, by applying the single relaxation time lattice Boltzmann method, the influences of nanoparticle concentration ϕ and the Rayleigh numbers Ra on heat transfer enhancement through Al_2O_3 -water nanofluid. This mixture is modeled as a unique phase within a square cavity, including a heated block with different forms (three aspect ratios). The principal findings of this work are as follows:

- The natural convection reduces with the decrease of nanoparticle concentrations ϕ , while it is enhanced as the Rayleigh number Ra increases.
- As nanoparticle concentrations ϕ rise and Rayleigh number Ra increases, the thermal conductivity increases, which increases the Nusselt number; therefore, the heat transfer of nanofluid improves.
- By raising the aspect ratio of the annulus AR_C , the Nusselt number calculated along the right surface of the inner square increases. Therefore, the heat transfer is enhanced. The Nu_{avg} is strongly affected for $AR_C = 0.75$.
- The heat transfer is enhanced in the case of the lowest aspect ratio of the obstacle ($AR_0 = 0.5$) in the outer square boundaries. While in the heated inner block, the heat transfer improvement depends on the interested surface.
- A rise in nanoparticle concentration parameter ϕ decreases the fluid velocity, but the temperature profiles increase. Also, with a rise of Rayleigh number Ra , the fluid velocity and convection process improve.
- The type of nanoparticles has an important effect on the natural convection heat transfer of nanofluids ($\text{TiO}_2/\text{Al}_2\text{O}_3$ -water): for Al_2O_3 , the natural

convection flow of nanofluid decreases, and the heat transfer increases, but for TiO_2 , both natural convection and heat transfer of nanofluid are enhanced.

REFERENCES

- [1] Ma, H., He, B., Su, L. and He, D.: Heat transfer enhancement of nanofluid flow at the entry region of microtubes, *Int. J. Therm. Sci.*, vol. 184, No. February 2022, 2023.
- [2] Khamlich, S., Jakobi, J., Khamliche, T. et al.: Enhanced heat transfer of laser-fabricated copper nanofluid at ultra-low concentration driven by the nanoparticle surface area, *J. Mol. Liq.*, vol. 383, p. 122104, Aug. 2023.
- [3] Babu, E. R., Reddy, N. C., Reddappa, H. N., Shivananda Murthy, K. V., Gnanendra Reddy, G. V. and Koppad, P. G.: Influence of Al_2O_3 nanoparticles on thermal performance of closed loop pulsating heat pipe, *FME Trans.*, vol. 48, No. 1, pp. 143–148, 2020.
- [4] Abed, I. M., Abdulkadhim, A., Hamzah, R. A., Hamzah, H. K. and Ali, F. H.: Natural convection heat transfer for adiabatic circular cylinder inside trapezoidal enclosure filled with nanofluid superposed porous-nanofluid layer, *FME Trans.*, vol. 48, No. 1, pp. 82–89, 2020.
- [5] Madhu, B., Bala Subramanian, E., Nagarajan, P. K., Sathyamurthy, R. and Mageshbabu, D.: Improving the yield of freshwater and exergy analysis of conventional solar still with different nanofluids, *FME Transactions*, vol. 45, No. 4, pp. 524–530, 2017.

- [6] Chen, Y., Wang, Z., He, J., Liu, X. and He, D.: Experimental analysis of electrical field combining nanofluids to enhance the mixed convective heat transfer in the rectangular channel, *Appl. Therm. Eng.*, vol. 227, p. 120432, Jun. 2023.
- [7] Ma, Y., Mohebbi, R., Rashidi, M. M. and Yang, Z.: Simulation of nanofluid natural convection in a U-shaped cavity equipped by a heating obstacle: Effect of cavity's aspect ratio, *J. Taiwan Inst. Chem. Eng.*, volume 93, pp. 263–276, December 2018.
- [8] Ma, Y., Mohebbi, R., Rashidi, M. M., Yang, Z.: Study of nanofluid forced convection heat transfer in a bent channel by means of lattice Boltzmann method, *Phys. Fluids*, vol. 30, No. 3, 2018.
- [9] Li, C. H. and Peterson, G. P.: Experimental studies of natural convection heat transfer of Al₂O₃/DI water nanoparticle suspensions (Nanofluids), *Adv. Mech. Eng.*, vol. 2010, 2010.
- [10] Hu, Y., He, Y., Qi, C., Jiang, B. and Inaki Schlaberg, H.: Experimental and numerical study of natural convection in a square enclosure filled with nanofluid, *Int. J. Heat Mass Transf.*, vol. 78, pp. 380–392, 2014.
- [11] Neves, F., Soares, A. A. and Rouboa, A.: Forced convection heat transfer of nanofluids in turbulent flow in a flat tube of an automobile radiator, *Energy Reports*, vol. 8, pp. 1185–1195, Nov. 2022.
- [12] Dong, C., Chen, S., Chen, R., Tian, W., Qiu, S., G. Su, H.: Numerical simulation of natural convection around the dome in the passive containment air-cooling system, *Nucl. Eng. Technol.*, Apr. 2023.
- [13] Wongchadukul, P., Datta, A. K., Rattanadecho, P.: Natural convection effects on heat transfer in a porous tissue in 3-D radiofrequency cardiac ablation, *Int. J. Heat Mass Transf.*, vol. 204, p. 123832, 2023.
- [14] Liu, W., Xu, G., Fu, Y., Wen, J., Zhang, N.: Numerical investigation on forced, natural, and mixed convective heat transfer of n-decane in laminar flow at supercritical pressures, *Int. J. Heat Mass Transf.*, vol. 209, 2023.
- [15] Li, Y., Liu, F., Li, X. and Jin, H.: Flow and heat transfer characteristics of natural convection in hydrothermal reactor with segmented heating, *Appl. Therm. Eng.*, vol. 227, p. 120451, Jun. 2023.
- [16] Habtay, G., Buzas, J. and Farkas, I.: Heat Transfer analysis in the chimney of the indirect solar dryer under natural convection mode, *FME Trans.*, vol. 48, No. 3, pp. 701–706, 2020.
- [17] Klazly, M., Mahabaleshwar, U. S. and Bognár, G.: Comparison of single-phase Newtonian and non-Newtonian nanofluid and two-phase models for convective heat transfer of nanofluid flow in backward-facing step, *J. Mol. Liq.*, vol. 361, p. 119607, Sep. 2022.
- [18] Hazeri-Mahmel, N., Shekari, Y. Tayebi, A.: Three-dimensional analysis of forced convection of Newtonian and non-Newtonian nanofluids through a horizontal pipe using single- and two-phase models, *Int. Commun. Heat Mass Transf.*, vol. 121, p. 105119, Feb. 2021.
- [19] Mohammadpour, J., Lee, A., Mozafari, M., Zargarabadi, M. R. and Mujumdar, A. S.: Evaluation of Al₂O₃-Water nanofluid in a microchannel equipped with a synthetic jet using single-phase and Eulerian–Lagrangian models, *Int. J. Therm. Sci.*, vol. 161, p. 106705, Mar. 2021.
- [20] Saha, G. and Paul, M. C.: Investigation of the characteristics of nanofluids flow and heat transfer in a pipe using a single phase model, *Int. Commun. Heat Mass Transf.*, vol. 93, pp. 48–59, 2018.
- [21] Dero, S., Rohni, A. M. and Saaban, A.: Stability analysis of Cu–C₆H₉NaO₇ and Ag–C₆H₉NaO₇ nanofluids with effect of viscous dissipation over stretching and shrinking surfaces using a single phase model, *Heliyon*, vol. 6, No. 3, p. e03510, Mar. 2020.
- [22] Abdollahzadeh, Y., Mehrpooya, M., Mousavian, S. M. A. and Moqtaderi, H.: Modeling and simulation of nanofluid in low Reynolds numbers using two-phase Lattice Boltzmann method based on mixture model, *Chem. Eng. Res. Des.*, vol. 192, pp. 402–411, 2023.
- [23] Akbari, O. A., Pourfattah, F., Mojaddarasil, M., Montazerifar, F., Masoumi, E. and Baghaei, S.: Assessing heat transfer and nanofluid laminar flow in the curved micro-mixers by adopting two-phase model, *Alexandria Eng. J.*, vol. 73, pp. 189–203, Jul. 2023.
- [24] Almitani, K. H., Alzaed, A., Alahmadi, A., Sharifpur, M. and Momin, M.: The influence of the geometric shape of the symmetrical twisted turbulator on the performance of parabolic solar collector having hybrid nanofluid: Numerical approach using two-phase model, *Sustain. Energy Technol. Assessments*, vol. 51, p. 101882, 2022.
- [25] Corina, A. N., Skorpa, R., Sangesland, S. Vrålstad, T.: Simulation of fluid flow through real micro-annuli geometries,” *J. Pet. Sci. Eng.*, vol. 196, p. 107669, Jan. 2021.
- [26] Termuhlen, R., Fitzmaurice, K. Yu, H.C.: Smoothed boundary method for simulating incompressible flow in complex geometries, *Comput. Methods Appl. Mech. Eng.*, vol. 399, p. 115312, Sep. 2022.
- [27] Ebrahimi, N., Ashtiani, H. A. D., and Toghraie, D.: Lattice Boltzmann method for mixed convection of nanofluid two-phase flow in a trapezoidal-shaped sinusoidal cavity by considering Brownian motion, *Eng. Anal. Bound. Elem.*, vol. 152, pp. 194–213, 2023.
- [28] Hssikou, M., Elguennouni, Y., Baliti, J., Alaoui, M.: Heat Transfer of Gas Flow within a Partially Heated or Cooled Square Cavity, *Model. Simul. Eng.*, vol. 2020, pp. 1–11, 2020.
- [29] Elguennouni, Y., Hssikou, M., Baliti, J., Ghafiri, R. Alaoui, M.: SRT-LBM and MRT-LBM comparison for a lid-driven gas microflow, *2020 1st Int. Conf. Innov. Res. Appl. Sci. Eng. Technol. IRASET 2020*, vol. 1, No. 1, 2020.

- [30] Baliti, J. et al.: Simulation of Natural Convection by Multirelaxation Time Lattice Boltzmann Method in a Triangular Enclosure, *Fluids*, vol. 7, No. 2, pp. 1–15, 2022.
- [31] Asha, N. E. J., Nag, P., Akhter, M. N. Molla, M. M.: MRT-lattice Boltzmann simulation of magnetic field effects on heat transfer from a heater in a C-shaped cavity filled with non-Newtonian hybrid nanofluids, *Int. J. Thermofluids*, vol. 18, p. 100345, May 2023.
- [32] Li, M., Qu, J., Ocloń, P., Wei, J. Tao, W.: 3D numerical simulation of condensation and condensate behaviors on textured structures using lattice Boltzmann method, *Int. J. Heat Mass Transf.*, vol. 160, p. 120198, 2020.
- [33] Chen, J., Dong, K., He, S., Deng, W., Zhao, J.: Investigation of biphilic microgroove surface on condensation Enhancement: A 3D Lattice Boltzmann method study, *Appl. Therm. Eng.*, vol. 219, p. 119520, 2023.
- [34] Brinkman, H. C.: The Viscosity of Concentrated Suspensions and Solutions, vol. 571, pp. 1–2, 1952.
- [35] Maxwell, J. C.: A treatise on electricity and magnetism, vol. 1. Clarendon press, 1873.
- [36] Zou, Q., He, X.: On pressure and velocity boundary conditions for the lattice Boltzmann BGK model, *Phys. Fluids*, vol. 9, No. 6, pp. 1591–1596, 1997.
- [37] Inamuro, T., Yoshino, M., Ogino, F.: A non-slip boundary condition for lattice Boltzmann simulations, *Phys. Fluids*, vol. 7, No. 12, pp. 2928–2930, 1995.
- [38] Mohamad, A. A.: Lattice Boltzmann Method, vol. 5, No. 5. 2010.
- [39] Arefmanesh, A., Amini, M., Mahmoodi, M., Najafi, M.: Buoyancy-driven heat transfer analysis in two-square duct annuli filled with a nanofluid, *Eur. J. Mech. - B/Fluids*, vol. 33, pp. 95–104, 2012.
- [40] Corvaro, F. and Paroncini, M.: Experimental analysis of natural convection in square cavities heated from below with 2D-PIV and holographic interferometry techniques, *Exp. Therm. Fluid Sci.*, vol. 31, No. 7, pp. 721–739, 2007.

NOMENCLATURE

AR_C	Annulus aspect ratio
AR_0	Obstacle aspect ratio
c_p	Specific heat capacity at constant pressure ($J.kg^{-1}.K^{-1}$)
c_i	Discrete vector of velocity in the i -direction ($m.s^{-1}$)
c_s	Speed of sound ($m.s^{-1}$)
f	The distribution function of density
f^{eq}	Equilibrium state of f
g	The distribution function of temperature
g^{eq}	The equilibrium state of g
Ma	Mach number
K	Thermal conductivity ($W.m^{-1}.K^{-1}$)
Nu	Local Nusselt number

Pr	Prandtl number
Ra	Rayleigh number
p	Pressure ($N.m^{-2}$)
L	Outer square length (m)
H	Obstacle height (m)
w	Obstacle width (m)
T	Normalized temperature
$\mathbf{u}(u,v)$	Vector of velocity ($m.s^{-1}$)
v_{scale}	Characteristic flow velocity ($m.s^{-1}$)
x,y	Cartesian coordinates

Greek symbols

ρ	Density ($kg.m^{-3}$)
α	Fluid thermal diffusivity ($m^2.s^{-1}$)
ν	Kinematic viscosity ($m^2.s^{-1}$)
β	Thermal expansion coefficient (K^{-1})
μ	Dynamic viscosity (Pa. s)
ω_i	Weight factors for flow and temperature (D_2Q_9)
ϕ	Nanoparticle volume fraction (%)
ψ	Stream (flow) function
τ_f	Relaxation time for flow(s)
τ_g	Relaxation time for temperature(s)
Δt	Time step (s)

Superscripts

f	Fluid
N_p	Solid nanoparticle
N_f	Nanofluid
avg	Average
H	Hot
C	Cold

NUMERICHO ISPITIVANJE PRENOSA TOPLOTE PRIRODNOM KONVEKCIJOM KORISHEENEM NANOFLUIDA TiO₂/Al₂O₃-VOДА

J. Oулаху, J. Елгенуни, M. Хсику, Ц. Балити, M. Алауи

Недавно су нанофлуиди коришћени као алтернатива у неколико индустрија за побољшање процеса преноса топлоте. Овај рад се фокусира на нумеричко моделирање перформанси процеса природне конвекције кроз нанофлуиде TiO₂/Al₂O₃-вода у квадратној шупљини која садржи загрејани блок. Решетка Болтзманнова метода је коришћена у овој студији за представљање побољшања преноса топлоте нанофлуида. Резултати су представљени у смислу струјних линија, изотермних контура и профила Нуселтовог броја. Налази показују да се повећањем Релејевог броја и концентрације чврстих наночестица повећава просечан Нуселтов број и откривају да загрејани блок енормно утиче на структуру протока и пренос топлоте. Такође је показано да врста наночестица значајно утиче на природни конвекцијски пренос топлоте.

